mater.scichina.com link.springer.com

Published online 4 July 2022 | https://doi.org/10.1007/s40843-022-2084-x
Sci China Mater 2022, 65(11): 3069–3076

Ultralow-concentration electrolyte boosting $K_{0.486}V_2O_5$ for high-performance proton storage

Shengyang Dong[1], Nan Lv[1], Ruiqi Ren[1], Yulin Wu[1], Pin Liu[1], Guoyin Zhu[1], Wenjun Wang[2], Yizhou Zhang[1*] and Xiaochen Dong[1,3*]

ABSTRACT High-concentration electrolytes are considered a promising tool for widening stable electrochemical windows and enhancing the electrochemical performance of aqueous batteries. However, their high cost, high viscosity, and low conductivity remain thorny issues. Because of the special Grotthuss mechanism of protons in water, proton batteries can use a low-concentration electrolyte to obtain sufficient kinetic performance. Herein, we present an unusual, ultralow-concentration sulfuric acid (0.01 mol L^{-1}) electrolyte to boost the electrochemical stability of K-ion pre-intercalated V_2O_5 ($K_{0.486}V_2O_5$, KVO). The KVO electrode exhibits a high reversible capacity of approximately 129 mA h g^{-1} at a low current density of 50 mA g^{-1} and impressive capacity retention of 78% over 20,000 cycles at 1 A g^{-1}. Ultralow-concentration electrolyte chemistry will open a novel route to exploit durable and low-cost aqueous energy storage systems.

Keywords: proton storage, ultralow-concentration electrolyte, Grotthuss mechanism, $K_{0.486}V_2O_5$, high stability

INTRODUCTION

Green and sustainable energy, notably wind power and solar energy, is emerging as a weapon against carbon dioxide emissions [1–3]. However, because of the indigenous properties of on-again and indeterminacy in the electrogenesis and consumption, a substantial demand-supply imbalance is needed for grid storage to couple the sustainable green energy systems. A high-efficiency energy storage system (ESS), particularly electrochemical energy storage (EES) technology, has great promise since it is less geographic and provides a modular solution [4–6]. In terms of large-scale application, the key parameters, including safety, cost, life span, energy density, and power density, are crucial for EES devices, particularly the first three parameters. Because of their low cost and internal security, aqueous rechargeable batteries (ARBs) occupy a unique position in the field of energy storage, particularly for grid-scale energy storage [7–9]. The research community has focused on earth-enriched metal ions, such as Na^+, K^+, Zn^{2+}, Mg^{2+}, and Al^{3+}, as the charge carriers [10–14]. In comparison, few researchers have considered nonmetallic ions. Given the large mass and radius of metal ions, a proton is an ideal charge carrier for rechargeable batteries because of its small radius, extensive availability, and low cost [15,16]. More importantly, protons can be transported through fast structural diffusion, which is the so-called Grotthuss mechanism [17,18]. In this transport mechanism, hydrogen bonding (H···O) and covalent bonding (H–O) switch between H_2O molecules, leading to the fast conduction of protons through the hydrogen-bonding network. In contrast, solvated metal ions diffuse individually through the electrolyte [19].

In general, tunnel-type or layered vanadium-based oxides are usually used as electrode materials for ARBs [20–25]. V_2O_5 is known for being slightly soluble in water, producing a yellowish acidic solution. The dissolution of V_2O_5 results in capacity fading due to the loss of active material. Most research has shown that guest ions or molecules (such as metal ions and water molecules) pre-intercalated into host structures of vanadium-based oxides can effectively alleviate the above problem and further improve the electrochemical properties [26–28]. For example, Kundu *et al.* [29] reported a double-layered $Zn_{0.25}V_2O_5{\cdot}nH_2O$ nanoribbon pre-embedded with Zn^{2+} and H_2O, which proved that the two guests can be used as "pillars" to substantially improve the zinc storage capacity and cyclic stability of V_2O_5.

In addition, the electrolyte concentration greatly influences electrochemical performance. Most research attention has focused on high-concentration electrolytes, especially in ARBs, because of the special interface and bulk structures in these solutions [30–32]. Although high-concentration electrolytes, particularly "water-in-salt" (WIS) electrolytes, have greatly widened the stable electrochemical window of aqueous electrolytes and enhanced electrochemical performance, they also bring problems like high cost, high viscosity, and low conductivity [33,34]. In contrast, little attention has been paid to low-concentration electrolytes. Although low ionic conductivity may cause concentration polarization, reducing the salt concentration to form an ultra-dilute electrolyte has not been explored [35,36]. Fortunately, because of the special Grotthuss mechanism of protons in water, proton batteries can use a dilute electrolyte to acquire sufficient kinetic performance.

Herein, we successfully demonstrate the efficacy of K-ion pre-intercalated V_2O_5 (KVO) as a favorable active material for proton storage in an ultralow-concentration electrolyte (i.e., 0.01 mol L^{-1} H_2SO_4), showing ultra-stable electrochemistry. The

[1] Institute of Advanced Materials and Flexible Electronics (IAMFE), School of Chemistry and Materials Science, Nanjing University of Information Science & Technology, Nanjing 210044, China
[2] School of Physical Science and Information Technology, Liaocheng University, Liaocheng 252059, China
[3] Key Laboratory of Flexible Electronics (KLOFE), Institute of Advanced Materials (IAM), Nanjing Tech University (NanjingTech), Nanjing 211816, China
* Corresponding authors (emails: yizhou.zhang@nuist.edu.cn (Zhang Y); iamxcdong@njtech.edu.cn (Dong X))

KVO cathode exhibits rapid ion migration and good structural stability in an aqueous electrolyte. When used as a positive electrode material, compared with metal ion (Na^+, K^+) electrolytes and other low-concentration acidic electrolytes, KVO delivers the highest reversible capacity of up to approximately 129 mA h g^{-1} at a current density of 50 mA g^{-1} in 0.01 mol L^{-1} H_2SO_4. More importantly, capacity retention of approximately 63% can be achieved after 50,000 cycles at 1 A g^{-1} in this low-concentration electrolyte.

EXPERIMENTAL SECTION

Synthesis of KVO

KVO was prepared *via* a general hydrothermal method according to the previous report [37]. Typically, 1 mmol V_2O_5 and 13.5 mmol KI were added to 30-mL deionized water under stirring. Then, 30-mmol KCl was added to the above mixed solution with continuous stirring for 1 h. Subsequently, this mixed solution was transferred to a 50-mL Teflon-lined stainless steel autoclave and heated to 200°C for 24 h. After hydrothermal growth, the precipitate was collected by centrifugation and washed several times with ethanol and deionized water. Finally, the obtained sample was dried in an oven at 80°C for 24 h.

Material characterization

The crystal structure was characterized on a Rigaku Ultra 250 with Cu Kα irradiation. The microscopic morphologies were characterized using field-emission scanning electron microscopy (FE-SEM, QUANTA 450) and transmission electron microscopy (TEM, JEOL JEM-2100F). A N_2 adsorption-desorption isotherm was collected on a Micromeritics ASAP2460 analyzer. X-ray photoelectron spectroscopy (XPS) analysis was performed on a Perkin-Elmer PHI 550 spectrometer with Al Kα (1486.6 eV) as the X-ray source. Thermogravimetric (TG) analysis was carried out on a TA STD650 thermal analyzer under N_2 atmosphere at a temperature ramp of 5°C min^{-1}.

Electrochemical measurement

The electrochemical measurements were conducted in a three-electrode Swagelok cell setup, where KVO on carbon paper was used as the working electrode, free-standing activated carbon (AC) film was used as the counter electrode, and a Ag/AgCl electrode (1 mol L^{-1} KCl) served as the reference electrode. The working electrode was prepared by mixing KVO, conductive agent acetylene black, and carboxymethyl cellulose (CMC) binder with a mass ratio of 7:2:1 in deionized water, where the homogeneous slurry was then cast onto the carbon paper. The active mass loading of the working electrode was approximately 1 mg cm^{-2}. An AC counter electrode was prepared by mixing AC, acetylene black, and polytetrafluoethylene (PTFE) with a mass ratio of 8:1:1 and a mass loading of approximately 20 mg cm^{-2}. AC was purchased from Kuraray™. We also used PTFE as the binder to prepare the free-standing films of the working electrodes for the *ex situ* X-ray diffraction (XRD), XPS, and TG measurements. All electrodes were dried at 60°C for 12 h under a vacuum. The filter paper was used as the separator. Notably, the surface area of the filter paper separator was only approximately 2 m^2 g^{-1} (Fig. S1a). The pore sizes were mainly distributed from 2 to 10 nm (Fig. S1b). Titanium rods were used as the negative electrode and positive electrode current collectors.

The full cell was assembled in a standard CR2032-type coin cell, where KVO was used as anode and cathode materials. The optimized mass ratio between anode and cathode was 1:1. All electrochemical measurements were performed at room temperature.

The energy density (E, W h kg^{-1}) and power density (P, W kg^{-1}) of the full cell can be obtained as follows [38,39]:

$$E = \int_{t_2}^{t_1} UI\,\mathrm{d}t, \tag{1}$$

$$P = E / \Delta t, \tag{2}$$

$$\Delta t = t_2 - t_1, \tag{3}$$

where I (A g^{-1}) is the current density normalized by the active mass in the cathode, t_1 and t_2 (h) are the starting and ending times of the discharge process, respectively, and U (V) is the voltage.

RESULTS AND DISCUSSION

Structural and morphology analysis

The as-prepared KVO was characterized by XRD to confirm its crystal structure. As shown in Fig. 1a, the XRD pattern matches well with monoclinic $K_{0.486}V_2O_5$ (JCPDS No. 86-0347) [40]. No significant peaks of other phases were detected, indicating the high purity of KVO. The inset of Fig. 1a shows the crystallographic arrangements of KVO along the *b*-axis. The structural framework consists of a bilayer network of edge-sharing twisted VO_6 octahedra, where the bilayers are stacked along the *c*-axis direction. K-ions are located between the V_2O_5 bilayers, forming a sandwich structure, which improves the reaction dynamics and reinforces the structural stability. Fig. 1b, c show the SEM images of KVO, where the nanorods are 100–150 nm wide and several micrometers long. This nanorod structure will shorten the ion diffusion distance, adapt to lattice strain, and improve the interface stability between the electrode and electrolyte. The detailed morphology of KVO was further investigated using TEM, which further reveals the nanorod structure (Fig. 1d). High-resolution TEM (HRTEM) reveals the (001) crystal plane of KVO with an interplanar distance of 0.95 nm (Fig. 1e), where the large interlayer may help accommodate the charge carrier. Furthermore, according to the N_2 adsorption/desorption isotherm (Fig. S2), KVO has a moderate surface area of approximately 21.8 m^2 g^{-1}. TG (Fig. 1f) and XRD (Fig. S3) data demonstrate the structural stability of KVO in water. XPS was used to analyze the elemental composition and valence state. As shown in Fig. S4a, the XPS survey spectrum proves the presence of K, V, and O elements, which demonstrates that K-ions are successfully embedded in V_2O_5 bilayers. The HR V $2p_{3/2}$ XPS result (Fig. S4b) shows that V is in the +4 (516.5 eV) and +5 (517.9 eV) valence states [41,42]. Notably, the peak area ratio of +5 and +4 is approximately 3.2, which further indicates that the K (i.e., V^{4+}) content of KVO is approximately 0.48.

Electrochemical performance of KVO

The proton storage performance of KVO was evaluated in a three-electrode cell setup with a potential window from 0 to 1.1 V (all three-electrode cell potentials hereafter are referred to as Ag/AgCl). From the galvanostatic charge-discharge (GCD) curves, the KVO electrode provides a reversible capacity of approximately 94 mA h g^{-1} at a current density of 100 mA g^{-1} in

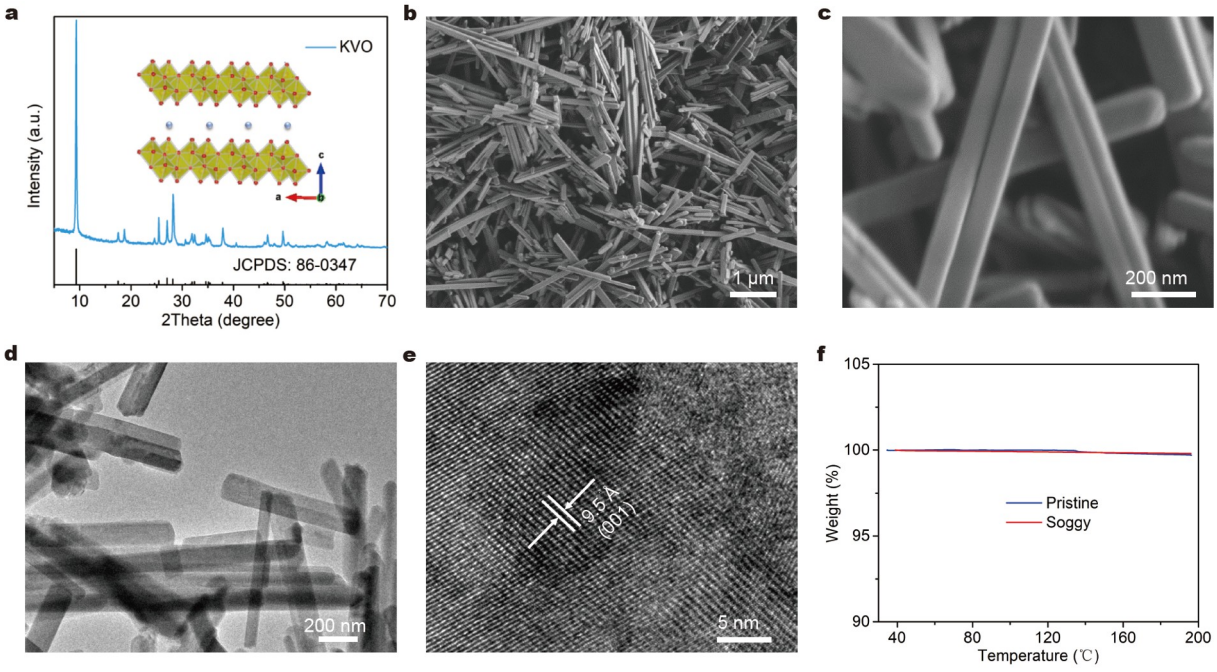

Figure 1 Physical characterization of KVO. (a) XRD pattern and crystal structure (inset) of KVO. SEM images (b, c) and TEM images (d, e) of KVO. (f) TG data of the as-prepared KVO before and after soaking in water for 3 h.

0.01 mol L^{-1} sulfuric acid electrolyte (Fig. 2a). As shown in Fig. 2b, when the current densities increase from 50 to 2000 mA g^{-1}, the corresponding discharge capacities are 129, 94, 81, 57, 40, and 31 mA h g^{-1}, respectively. In addition, the KVO electrode also possesses outstanding cycling stability, with a 78% capacity retention at 20,000 cycles and 53% at 50,000 cycles under a current density of 1 A g^{-1} (Fig. 2c). Moreover, the proton storage in carbon paper is very limited, as demonstrated by the cyclic voltammetry (CV) curves of carbon paper and KVO electrodes in Fig. S5. We also tested the electrochemical performance of V_2O_5 in 0.01 mol L^{-1} H_2SO_4 electrolyte. As shown in Fig. S6, the electrochemical performance of V_2O_5 is far inferior to that of KVO. For example, the specific capacity of V_2O_5 is only approximately 30 mA h g^{-1} at 50 mA g^{-1}. The results indicate that the electrochemical properties of V_2O_5 materials will be substantially improved by the pre-embedded K-ions.

Subsequently, a series of sulfuric acid electrolytes with different concentrations were used to investigate the significance of concentration. In Fig. 2d, e, the KVO electrode has the best rate capability in 0.01 mol L^{-1} sulfuric acid. Although the initial capacity (~143 mA h g^{-1}) is the highest using the 0.1 mol L^{-1} electrolyte at a low current density of 50 mA g^{-1}, the capacity of ~20 mA h g^{-1} is the lowest among the various concentrations of electrolyte at subsequent 100 mA g^{-1}, indicating an unstable structure (Fig. S7) and cycling performance under a relatively high acidic condition. The limited proton storage capacity in the lower concentration electrolyte solutions is due to the low ionic conductivity. Fig. S8 further compares the electrochemical performance of the KVO electrode using the same concentration of electrolyte solution (0.01 mol L^{-1}) with different cations (H^+, Na^+, and K^+). At 50 mA g^{-1}, KVO electrodes deliver similar capacities of only approximately 30 mA h g^{-1} in 0.01 mol L^{-1} Na_2SO_4 and K_2SO_4 electrolytes. As shown in Fig. S8b, 0.01 mol L^{-1} H_2SO_4 exhibits the best rate capacity among the aforementioned three cationic electrolytes. Therefore, 0.01 mol L^{-1} H_2SO_4 is the optimal electrolyte and is selected for the following analysis.

Energy storage mechanism analysis

To determine whether H_2O is co-intercalated or de-intercalated into or out of the structure of KVO with proton, we conducted TG analysis. Notably, according to Fig. 1f and Fig. S9, over the first charge with the K-ion de-intercalated out from KVO, the additional lattice water is absorbed into the structure of KVO. During the first protonation, some lattice water is expelled from KVO. Therefore, the migration direction of H_2O is opposite to that of charge carriers. The overall result is naked proton intercalation rather than hydronium ion insertion in the initial protonation process. The complicated migration process of charge carriers needs further probing in the future.

To explore the evolution of the KVO crystalline structure during GCD, we conducted *ex situ* XRD studies during the first cycle (Fig. 3a–c). As shown in Fig. 3b, the main peaks shift to a lower degree after de-potassiation, suggestive of structural expansion along the *c*-axis. Upon protonation to 0 V, the main peaks gradually return to a higher degree. Notably, the evolution of the (001) diffraction peaks (Fig. 3c) is particularly interesting. When the KVO electrode is incipiently charged to 0.9 V, the (001) peak shifts to the left obviously, which may be due to the large amount of water intercalation with increasing layer spacing. In addition, interestingly, when the electrode is continuously charged to 1.1 V, the (001) peak only moves to a slightly lower angle, which is indicative of the relative trade-off between the effects of K-ion de-intercalation and water intercalation. When the KVO electrode is gradually discharged from 1.1 to 0 V, the (001) peak shifts to the right, but it does not return to the initial position. This phenomenon is mainly due to

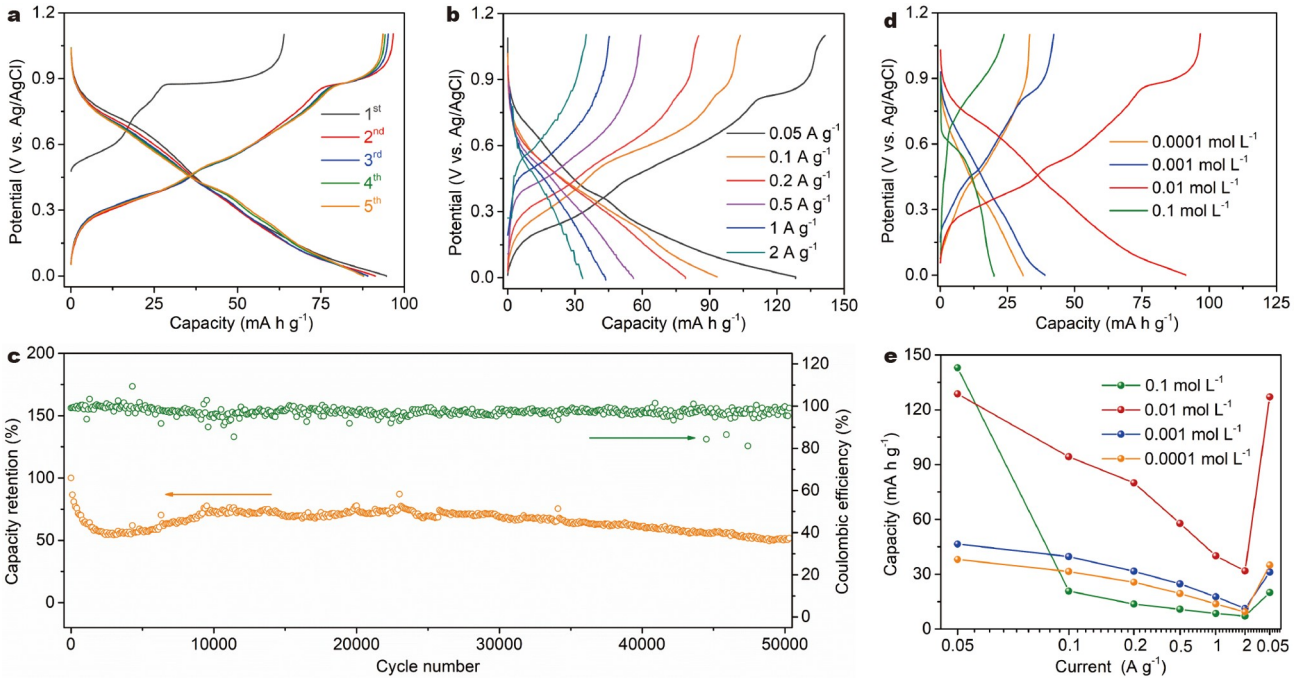

Figure 2 Electrochemical characterization of the KVO electrode. (a) First five GCD curves at a current density of 100 mA g^{-1} in 0.01 mol L^{-1} electrolyte. (b) Typical GCD curves in 0.01 mol L^{-1} electrolyte from 0.05 to 2 A g^{-1}. (c) Cycling stability in 0.01 mol L^{-1} electrolyte at a current density of 1 A g^{-1}. (d) Typical GCD curves in different concentrations of sulfuric acid electrolyte solution at 100 mA g^{-1}. (e) Rate performance in different concentrations of sulfuric acid electrolyte.

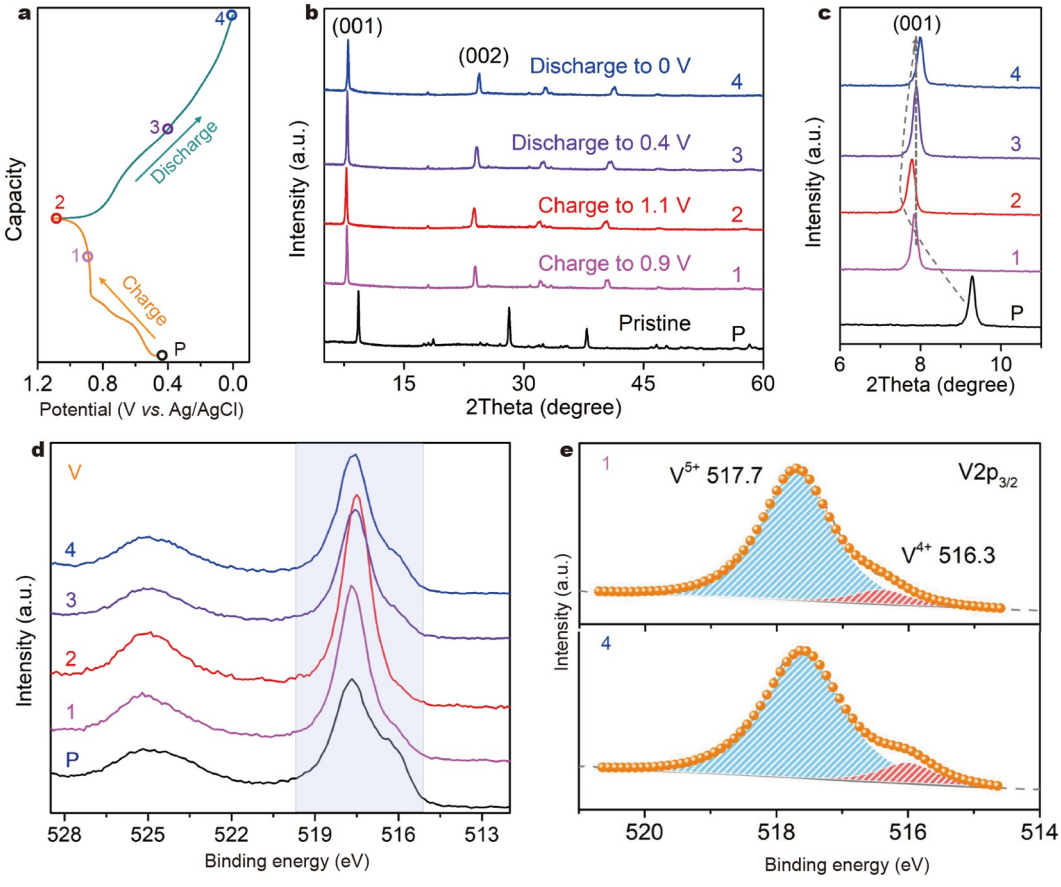

Figure 3 (a) GCD curves of the KVO electrode at 0.1 A g^{-1}. (b) *Ex situ* XRD patterns of the KVO electrode under different charge and discharge states. (c) Evolution of the (001) peak of the KVO electrode. (d, e) *Ex situ* XPS spectra of the KVO electrode at selected SOCs.

the residual water between bilayers, which is consistent with the results of TG in Fig. S9. We further conducted *ex situ* XPS to study the valence state of V in KVO during the first GCD (Fig. 3d, e). All V $2p_{3/2}$ spectra are deconvoluted into two peaks with binding energies at 517.9 and 516.5 eV, corresponding to V^{5+} and V^{4+}, respectively. When the KVO electrode is initially charged to 1.1 V gradually, the V^{5+} signal increases, and the V^{4+} signal decreases. This result demonstrates that some V^{4+} is oxidized to V^{5+} during the charging process. Subsequently, while the KVO electrode is discharged to 0 V, some V^{5+} is reduced to V^{4+} again, resulting in a decrease in the V^{5+} signal and an increase in the V^{4+} signal. As shown in Fig. 3e, the valence state of V returns to the original state after full protonation, further demonstrating the high reversibility of the electrochemical reaction.

Kinetic analysis of KVO

To further detect the kinetics of the KVO electrode for proton storage, CV curves were obtained with scanning rates from 2 to 6 mV s^{-1}. As shown in Fig. 4a, the CV curves show similar shapes with increasing scan rates, which indicates the good electrochemical reversibility of KVO. The capacity contributed in CV can be deconvoluted into two portions: the diffusion-controlled part and the capacitive non-diffusion-controlled part [43–45]. These two behaviors obey the equation $I = av^b$, where i (A g^{-1}) represents the CV current, a and b are coefficients, and v (mV s^{-1}) is the scan rate. The obtained b value then indicates the charge storage type. b = 0.5 suggests a diffusion-controlled process, whereas b = 1 indicates capacitive behavior. As shown in Fig. 4b, b ranges from 0.7 to 0.8, implying that the charge storage process is diffusion and capacitive (non-diffusion) co-controlled. Furthermore, the specific contribution of capacitive capacity at different scan rates can be calculated as $i = k_1v + k_2v^{1/2}$, where k_1v is the capacitive contribution, and $k_2v^{1/2}$ is the diffusion-controlled part. Under this mathematical treatment, the contribution of capacitive storage is approximately 51% at 6 mV s^{-1} (Fig. 4c). As demonstrated in Fig. 4d and Fig. S10, the contribution of capacitive storage gradually increases as the scan rate increases.

The galvanostatic intermittent titration technique (GITT) was applied to further study the diffusion kinetics of KVO (Fig. 4e, f, and Fig. S11). Fig. 4e shows the evolving diffusion coefficients as a function of the state of charge (SOC), where the calculated diffusion coefficient is approximately 10^{-11}–10^{-8} cm^2 s^{-1} (Fig. 4f), indicating the fast diffusion of charge carriers in the KVO electrode.

Electrochemical performance of the full cell

To evaluate the practicability, we further fabricated a full cell with KVO as the anode and cathode materials. According to the electrochemical performance of the KVO anode (Fig. S12), between −0.8 and 0 V in 0.01 mol L^{-1} H_2SO_4 electrolyte, the optimized mass ratio between the anode and cathode should be 1:1. Before assembling the full cell, the KVO electrode needs to be pre-activated by cycling three times at 0.1 A g^{-1}. Fig. 5a shows the full cell's configuration based on the KVO electrode as the anode and cathode. The additional lattice water and terminal oxygen in KVO form a hydrogen-bonding network for fast Grotthuss proton conduction during the charging and discharging. As shown in Fig. 5b, the full cell exhibits a discharge capacity of approximately 83 mA h g^{-1} (~3000 s) based on the mass of one electrode between 0 and 1.7 V at 0.1 A g^{-1}. The

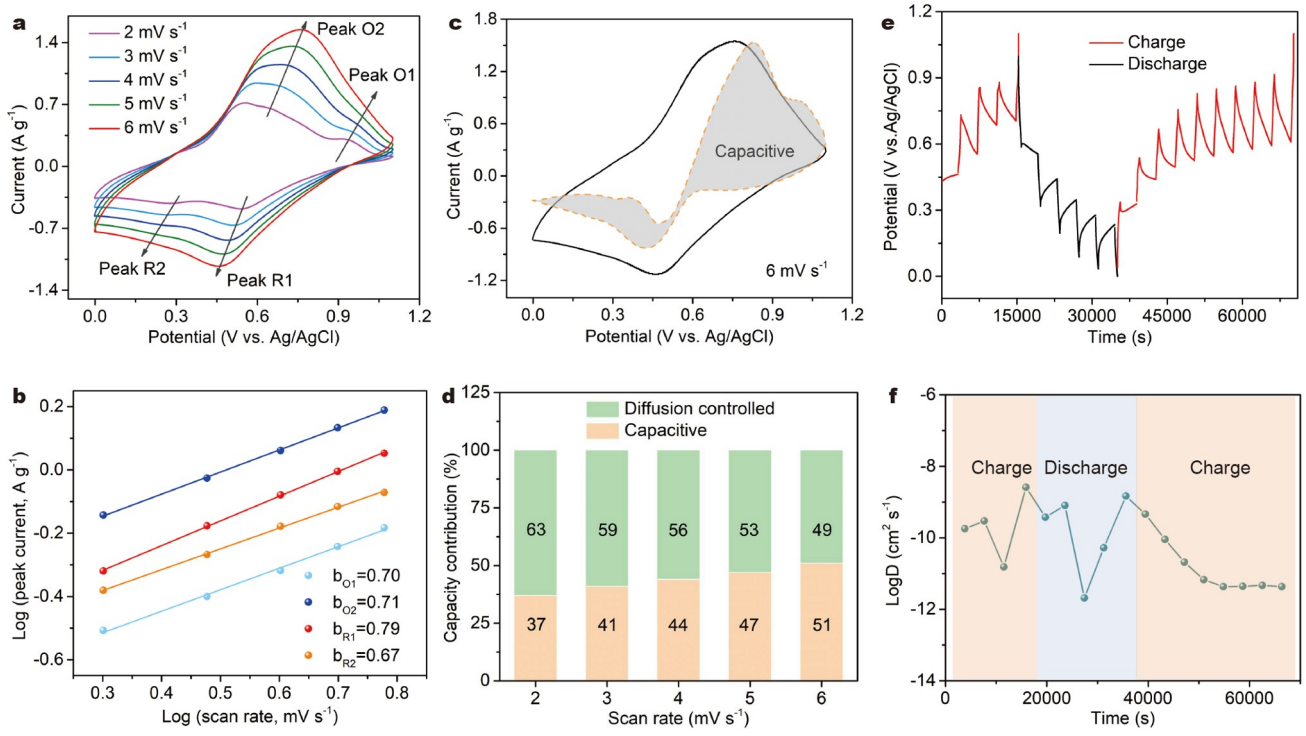

Figure 4 Kinetic analysis of the KVO electrode. (a) CV curves of the KVO electrode at different scan rates. (b) log(i) *vs.* log(v) plots at redox peaks. (c) Capacitive contribution displayed in the shaded section evaluated at a scan rate of 6 mV s^{-1}. (d) Contribution percentage of diffusion-controlled capacities and capacitive capacities. (e) GCD curves in the GITT measurement (0.1 A g^{-1} for 10 min followed by a 1-h rest) and (f) the corresponding proton diffusion coefficient.

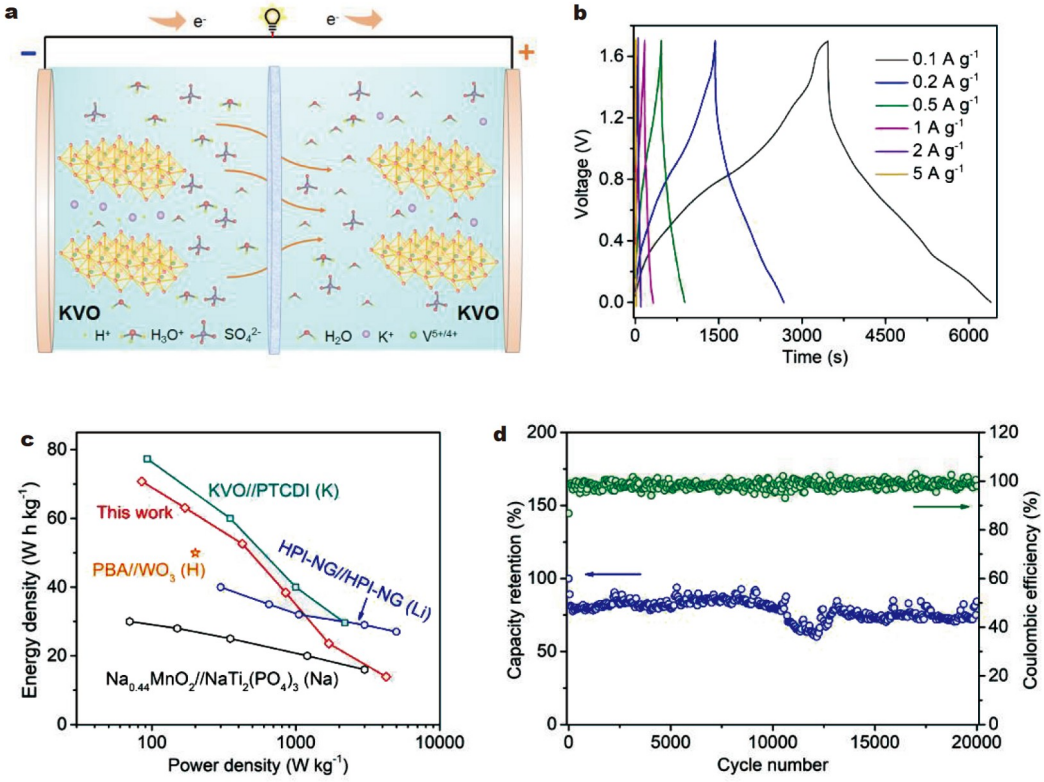

Figure 5 Electrochemical evaluation of the KVO//KVO full cell. (a) Diagrammatic sketch of the electrochemical reaction process during the discharge. (b) GCD curves at different current densities between 0 and 1.7 V. (c) Ragone plots of KVO//KVO and other aqueous batteries. (d) Capacity retention and Coulombic efficiency on 20,000 cycles at a current density of 1 A g^{-1}.

Ragone plot (Fig. 5c) obtained from rate performance (Fig. 5b) demonstrates the considerable energy and power output of the designed full cell. A high energy density of 71 W h kg^{-1} is achieved at a power density of 85 W kg^{-1}. The full cell still provides an energy density of 14 W h kg^{-1}, even at a high power density of 4250 W kg^{-1}. Compared with previously reported aqueous proton and metal-ion batteries with conventional electrolytes, such as PBA//WO_3 (H) [19], HPI-NG//HPI-NG (Li) [46], $Na_{0.44}MnO_2$//$NaTi_2(PO_4)_3$ (Na) [10], and KVO//PTCDI (K) [21], the KVO//KVO full cell based on ultralow-concentration acid electrolyte has comparable energy and power characteristics. In addition, the long cycling characteristic of the full cell (see Fig. 5d) was conducted at a current density of 1 A g^{-1}. The capacity retention is approximately 84% after 20,000 cycles, which is comparable to other aqueous nonmetallic charge carrier batteries, such as the CuFe PBA//Cu battery (H; 85.2% after 5000 cycles) [47] and CuFe PBA//h-MoO_3 (NH_4; 92.4% after 2000 cycles) [48]. The superior electrochemical characteristics of KVO can be attributed to the following aspects. First, the well-organized nanorod structure optimizes and shortens the transmission route of protons and electrons. Second, the moderate acid electrolyte benefits structural stability. Moreover, the hydrogen-bonding network of lattice water molecules inside the de-potassiation KVO structure facilitates the fast Grotthuss proton conduction.

CONCLUSIONS

In summary, we successfully demonstrate that KVO can work well in ultralow-concentration acid electrolytes (0.01 mol L^{-1} H_2SO_4). The dilute electrolyte not only decreases the acid aggressiveness but also substantially reduces the cost, resulting in stable proton storage and low cost. KVO delivers high proton storage capacity (~129 mA h g^{-1} at 50 mA g^{-1}) and impressive cycling stability (53% capacity retention after 50,000 cycles) between 0 and 1.1 V in ultralow-concentration acid electrolytes. More importantly, the repulsion and intercalation of water have been found during the charge and discharge process. The dilute electrolyte chemistry for proton storage can be extended to other ESSs for large-scale energy storage fields.

Received 1 March 2022; accepted 15 April 2022; published online 4 July 2022

1 Shi X, Sun Y, Shen Y. China's ambitious energy transition plans. Science, 2021, 373: 170
2 Mallapaty S. How China could be carbon neutral by mid-century. Nature, 2020, 586: 482–483
3 Larcher D, Tarascon JM. Towards greener and more sustainable batteries for electrical energy storage. Nat Chem, 2015, 7: 19–29
4 Hou S, Ji X, Gaskell K, *et al.* Solvation sheath reorganization enables divalent metal batteries with fast interfacial charge transfer kinetics. Science, 2021, 374: 172–178
5 Usiskin R, Lu Y, Popovic J, *et al.* Fundamentals, status and promise of sodium-based batteries. Nat Rev Mater, 2021, 6: 1020–1035
6 Wu L, Dong S, Pang G, *et al.* Rocking-chair Na-ion hybrid capacitor: A high energy/power system based on $Na_3V_2O_2(PO_4)_2F$@PEDOT core-shell nanorods. J Mater Chem A, 2019, 7: 1030–1037
7 Ruan P, Liang S, Lu B, *et al.* Design strategies for high-energy-density aqueous zinc batteries. Angew Chem Int Ed, 2022, 61: e202200598
8 Yuan X, Ma F, Zuo L, *et al.* Latest advances in high-voltage and high-energy-density aqueous rechargeable batteries. Electrochem Energ Rev,

2021, 4: 1–34
9 Chao D, Zhou W, Xie F, *et al.* Roadmap for advanced aqueous batteries: From design of materials to applications. Sci Adv, 2020, 6: eaba4098
10 Guo Z, Zhao Y, Ding Y, *et al.* Multi-functional flexible aqueous sodium-ion batteries with high safety. Chem, 2017, 3: 348–362
11 Charles DS, Feygenson M, Page K, *et al.* Structural water engaged disordered vanadium oxide nanosheets for high capacity aqueous potassium-ion storage. Nat Commun, 2017, 8: 15520
12 Li Z, An Y, Dong S, *et al.* Progress on zinc ion hybrid supercapacitors: Insights and challenges. Energy Storage Mater, 2020, 31: 252–266
13 Dong H, Tutusaus O, Liang Y, *et al.* High-power Mg batteries enabled by heterogeneous enolization redox chemistry and weakly coordinating electrolytes. Nat Energy, 2020, 5: 1043–1050
14 Yan C, Lv C, Wang L, *et al.* Architecting a stable high-energy aqueous Al-ion battery. J Am Chem Soc, 2020, 142: 15295–15304
15 Wang X, Bommier C, Jian Z, *et al.* Hydronium-ion batteries with perylenetetracarboxylic dianhydride crystals as an electrode. Angew Chem Int Ed, 2017, 56: 2909–2913
16 Guo Z, Huang J, Dong X, *et al.* An organic/inorganic electrode-based hydronium-ion battery. Nat Commun, 2020, 11: 959
17 Agmon N. The Grotthuss mechanism. Chem Phys Lett, 1995, 244: 456–462
18 Gileadi E, Kirowa-Eisner E. Electrolytic conductivity—The hopping mechanism of the proton and beyond. Electrochim Acta, 2006, 51: 6003–6011
19 Wu X, Hong JJ, Shin W, *et al.* Diffusion-free Grotthuss topochemistry for high-rate and long-life proton batteries. Nat Energy, 2019, 4: 123–130
20 He P, Zhang G, Liao X, *et al.* Sodium ion stabilized vanadium oxide nanowire cathode for high-performance zinc-ion batteries. Adv Energy Mater, 2018, 8: 1702463
21 Liang G, Gan Z, Wang X, *et al.* Reconstructing vanadium oxide with anisotropic pathways for a durable and fast aqueous K-ion battery. ACS Nano, 2021, 15: 17717–17728
22 Fu Q, Wang J, Sarapulova A, *et al.* Electrochemical performance and reaction mechanism investigation of V_2O_5 positive electrode material for aqueous rechargeable zinc batteries. J Mater Chem A, 2021, 9: 16776–16786
23 Lei K, Zhu Z, Yin Z, *et al.* Dual interphase layers *in situ* formed on a manganese-based oxide cathode enable stable potassium storage. Chem, 2019, 5: 3220–3231
24 Guan C, Hu F, Yu X, *et al.* High performance of $HNaV_6O_{16}{\cdot}4H_2O$ nanobelts for aqueous zinc-ion batteries with *in-situ* phase transformation by $Zn(CF_3SO_3)_2$ electrolyte. Rare Met, 2022, 41: 448–456
25 Gu ZY, Guo JZ, Cao JM, *et al.* An advanced high-entropy fluorophosphate cathode for sodium-ion batteries with increased working voltage and energy density. Adv Mater, 2022, 34: 2110108
26 Yan M, He P, Chen Y, *et al.* Water-lubricated intercalation in $V_2O_5{\cdot}nH_2O$ for high-capacity and high-rate aqueous rechargeable zinc batteries. Adv Mater, 2018, 30: 1703725
27 Yang Y, Tang Y, Fang G, *et al.* Li^+ intercalated $V_2O_5{\cdot}nH_2O$ with enlarged layer spacing and fast ion diffusion as an aqueous zinc-ion battery cathode. Energy Environ Sci, 2018, 11: 3157–3162
28 Huang J, Zhou J, Liang S. Guest pre-intercalation strategy to boost the electrochemical performance of aqueous zinc-ion battery cathodes. Acta Physico Chim Sin, 2020, 0: 2005020–0
29 Kundu D, Adams BD, Duffort V, *et al.* A high-capacity and long-life aqueous rechargeable zinc battery using a metal oxide intercalation cathode. Nat Energy, 2016, 1: 16119
30 Suo L, Borodin O, Gao T, *et al.* "Water-in-salt" electrolyte enables high-voltage aqueous lithium-ion chemistries. Science, 2015, 350: 938–943
31 Dong S, Wang Y, Chen C, *et al.* Niobium tungsten oxide in a green water-in-salt electrolyte enables ultra-stable aqueous lithium-ion capacitors. Nano-Micro Lett, 2020, 12: 168
32 Lukatskaya MR, Feldblyum JI, Mackanic DG, *et al.* Concentrated mixed cation acetate "water-in-salt" solutions as green and low-cost high voltage electrolytes for aqueous batteries. Energy Environ Sci, 2018, 11: 2876–2883
33 Jiang LL, Yan C, Yao YX, *et al.* Inhibiting solvent co-intercalation in a graphite anode by a localized high-concentration electrolyte in fast-charging batteries. Angew Chem Int Ed, 2021, 60: 3402–3406
34 Jaumaux P, Yang X, Zhang B, *et al.* Localized water-in-salt electrolyte for aqueous lithium-ion batteries. Angew Chem Int Ed, 2021, 60: 19965–19973
35 Li Y, Yang Y, Lu Y, *et al.* Ultralow-concentration electrolyte for Na-ion batteries. ACS Energy Lett, 2020, 5: 1156–1158
36 Kim DH, Hwang S, Cho JJ, *et al.* Toward fast operation of lithium batteries: Ion activity as the factor to determine the concentration polarization. ACS Energy Lett, 2019, 4: 1265–1270
37 Deng L, Niu X, Ma G, *et al.* Layered potassium vanadate $K_{0.5}V_2O_5$ as a cathode material for nonaqueous potassium ion batteries. Adv Funct Mater, 2018, 28: 1800670
38 Wang H, Zhu C, Chao D, *et al.* Nonaqueous hybrid lithium-ion and sodium-ion capacitors. Adv Mater, 2017, 29: 1702093
39 Zhang Y, An Y, Yin B, *et al.* A novel aqueous ammonium dual-ion battery based on organic polymers. J Mater Chem A, 2019, 7: 11314–11320
40 Li L, Liu S, Liu W, *et al.* Electrolyte concentration regulation boosting zinc storage stability of high-capacity $K_{0.486}V_2O_5$ cathode for bendable quasi-solid-state zinc ion batteries. Nano-Micro Lett, 2021, 13: 34
41 Zhu K, Zhang C, Guo S, *et al.* Sponge-like cathode material self-assembled from two-dimensional V_2O_5 nanosheets for sodium-ion batteries. ChemElectroChem, 2015, 2: 1660–1664
42 Dong S, Shin W, Jiang H, *et al.* Ultra-fast NH_4^+ storage: Strong H bonding between NH_4^+ and bi-layered V_2O_5. Chem, 2019, 5: 1537–1551
43 Wang J, Polleux J, Lim J, *et al.* Pseudocapacitive contributions to electrochemical energy storage in TiO_2 (anatase) nanoparticles. J Phys Chem C, 2007, 111: 14925–14931
44 Kim HS, Cook JB, Lin H, *et al.* Oxygen vacancies enhance pseudocapacitive charge storage properties of MoO_{3-x}. Nat Mater, 2017, 16: 454–460
45 Chao D, Ouyang B, Liang P, *et al.* C-plasma of hierarchical graphene survives SnS bundles for ultrastable and high volumetric Na-ion storage. Adv Mater, 2018, 30: 1804833
46 Zhao Y, Liu J, Zheng D, *et al.* Achieving high capacitance of paper-like graphene films by adsorbing molecules from hydrolyzed polyimide. Small, 2018, 14: 1702809
47 Liang G, Mo F, Yang Q, *et al.* Commencing an acidic battery based on a copper anode with ultrafast proton-regulated kinetics and superior dendrite-free property. Adv Mater, 2019, 31: 1905873
48 Liang G, Wang Y, Huang Z, *et al.* Initiating hexagonal MoO_3 for superb-stable and fast NH_4^+ storage based on hydrogen bond chemistry. Adv Mater, 2020, 32: 1907802

Acknowledgements This work was supported by the National Natural Science Foundation of China (52102264), the Natural Science Foundation of Jiangsu Province (BK20200826), the Natural Science Foundation of Jiangsu Higher Education Institutions (20KJB430018), the Startup Foundation for Introducing Talent of NUIST (2020r023), and Jiangsu Provincial Scientific Research and Practice Innovation Program (KYCX21_0991).

Author contributions All authors contributed to the writing of this paper. All authors have given approval to the final version of the paper. Dong S contributed the idea; Lv N and Ren R prepared the materials and performed the experiments; Wu Y, Liu P, and Zhu G finished the physical characterization; Dong S and Lv N wrote the paper; Zhang Y and Dong X supervised the revision of the paper.

Conflict of interest The authors declare that they have no conflict of interest.

Supplementary information Supporting data are available in the online version of the paper.

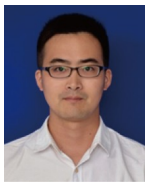

Sheng-Yang Dong received his PhD degree in 2019 from Nanjing University of Aeronautics and Astronautics (NUAA), China, and then joined Nanjing University of Information Science and Technology (NUIST). His current research mainly focuses on developing advanced materials for sustainable energy storage, such as aqueous batteries, hybrid capacitors, Na/K-ion batteries, and dual-ion batteries.

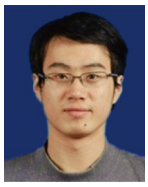

Yi-Zhou Zhang received his bachelor's degree from Nanjing University, and obtained a PhD degree from Nanjing University of Posts & Telecommunications under the supervision of Prof. Wei Huang. He is now a professor of materials science and engineering at NUIST. He mainly works on functional materials for printed and flexible energy storage and electronics.

Xiao-Chen Dong obtained his PhD degree from Zhejiang University, China, in 2007. He then joined the School of Materials Science and Engineering at Nanyang Technological University as a postdoctoral research associate. In 2012, he joined the Institute of Advanced Materials, Nanjing Tech University, as a full professor. His current research mainly focuses on flexible electronics and biophotonics.

超低浓度电解液助力$K_{0.486}V_2O_5$高性能质子存储

董升阳[1], 吕南[1], 任睿祺[1], 吴雨琳[1], 刘品[1], 朱国银[1], 王文军[2], 张一洲[1*], 董晓臣[1,3*]

摘要 高浓度电解液被认为是一种很有前景的拓宽电解液电化学稳定窗口和提高水系电池电化学性能的方法. 但是高浓度电解液也存在高成本、高粘度、低电导率等棘手问题. 因为特殊的Grotthuss机制, 质子电池能够在低浓度电解液中获得足够的动力学性能. 基于此, 我们采用罕见的超低浓度硫酸电解液(0.01 mol L^{-1})助力K^+预嵌的V_2O_5($K_{0.486}V_2O_5$, KVO)电化学稳定性. 在50 mA g^{-1}的低电流密度下, KVO电极具有129 mA h g^{-1}的比容量; 在1 A g^{-1}的电流密度下, 循环20,000圈的容量保持率为78%. 超低浓度电解液策略为开拓耐用的、低成本的水系能源存储系统提供了一种新的路径.

